



LAWRENCE
LIVERMORE
NATIONAL
LABORATORY

Characterization of a picosecond laser generated 4.5 keV Ti K-alpha source for pulsed radiography

J. A. King, M. H. Key, C. D. Chen, R. R. Freeman, T. Phillips, K. U. Akli, M. Borghesi, M. Chen, T. Cowan, S. Hatchett, J. A. Koch, K. L. Lancaster, A. MacKinnon, C. D. Murphy, P. Norreys, P. Patel, L. Romagnani, R. Snavely, R. Stephens, C. Stoeckl, R. Town, M. Zepf, B. Zhang

March 25, 2005

Review of Scientific Instruments

Disclaimer

This document was prepared as an account of work sponsored by an agency of the United States Government. Neither the United States Government nor the University of California nor any of their employees, makes any warranty, express or implied, or assumes any legal liability or responsibility for the accuracy, completeness, or usefulness of any information, apparatus, product, or process disclosed, or represents that its use would not infringe privately owned rights. Reference herein to any specific commercial product, process, or service by trade name, trademark, manufacturer, or otherwise, does not necessarily constitute or imply its endorsement, recommendation, or favoring by the United States Government or the University of California. The views and opinions of authors expressed herein do not necessarily state or reflect those of the United States Government or the University of California, and shall not be used for advertising or product endorsement purposes.

Characterization of a Picosecond Laser Generated 4.5 keV Ti K-alpha Source for Pulsed Radiography

J.A.King³, M.H.Key¹, C.D.Chen¹, R.R.Freeman^{3,8}, T.Phillips¹, K.Akli³, M.Borghesi⁵, M.Chen¹, T.Cowan⁴, S.Hatchett¹, J.A.Koch¹, K.L.Lancaster^{2,7}, A.J.MacKinnon¹, C.D.Murphy^{2,7}, P.Norreys², P.K.Patel¹, L.Romagnani⁵, R.Snavely³, R.Stephens⁴, C.Stoeckl⁶, R.P.J.Town¹, M.Zepf⁵, B.Zhang³

¹Lawrence Livermore National Laboratory, Livermore, CA, USA

²Rutherford Appleton Laboratory, Chilton, Oxon, UK

³University of California, Davis, Davis, CA, USA

⁴General Atomics, San Diego, CA, USA

⁵The Queen's University of Belfast, Belfast, UK

⁶University of Rochester-LLE, Rochester, NY, USA

⁷The Blackett Laboratory, Imperial College, London, UK

⁸The Ohio State University, Columbus, Ohio 43210, USA

K α radiation generated by interaction of an ultra-short (1ps) laser with thin (25 μm) Ti foils at high intensity ($2 \times 10^{16} \text{ W/cm}^2$) is analyzed using data from a spherical Bragg crystal imager and a single hit CCD spectrometer together with Monte-Carlo simulations of K α brightness. Laser to K α and electron conversion efficiencies have been determined. We have also measured an effective crystal reflectivity of $3.75 \pm 2\%$. Comparison of imager data with data from the relatively broadband single hit spectrometer has revealed a reduction in crystal collection efficiency for high K α yield. This is attributed to a shift in the K-shell spectrum due to Ti ionization.

Recently, a first demonstration was made of radiography of implosions using a non-thermal K α radiation source, generated with a high intensity picosecond laser pulse¹. This technique gives more than a 10-fold improvement in time resolution over thermal x-ray radiography and readily achieves the brightness required for high definition radiography. The absolute source brightness is important in assessing the potential of this diagnostic and we present here measurements and Monte-Carlo simulations of the brightness of the Ti K α back-lighter source.

The experiment was conducted at the Vulcan laser within the Rutherford Appleton Laboratory in the UK. A back-lighting source was produced using a chirped pulse amplified (CPA) beam (1 ps, 49J average on target) normally incident on a 25 micron thick Ti foil and defocused to an elliptical spot with major and minor FWHM diameters of 0.8 mm and 0.4 mm. The average intensity on foil was $1.9 \times 10^{16} \text{ W/cm}^2$ with an average peak intensity of $2.5 \times 10^{16} \text{ W/cm}^2$. The target was exposed to amplified spontaneous emission (ASE) and leakage pre-pulse at $<10^{-7}$: 1 intensity contrast and 10^{-4} : 1 energy contrast in a few nanosecond window prior to the main pulse.

Two instruments were used to characterize the K α source. The first was a spherical Bragg crystal imager (quartz 2023, 2d of 0.2749 nm, radius of curvature 38cm, apertured to 1.6 cm) used to spatially resolve the emission of the K α back-lighter source². The crystal focused the 4.5 keV K α photons with 10 μm spatial resolution and 7.9x magnification onto a cooled 16-bit, 1" square, 1024x1024 pixel CCD chip. The observation

angle was normal to the rear axis of the foil. A 10 μm thick Ti foil further filtered the Ti K α radiation. Figure 1 shows a typical image. A single hit CCD spectrometer measured the absolute K α yield from the Ti target. It consisted of a back-thinned CCD with 2048x2048, 13.5 μm square pixels and a filter (100 or 150 micron Ti) that placed the chip in the single hit photon regime. The angle of observation was 41 $^\circ$ from the rear surface normal of the Ti foil.

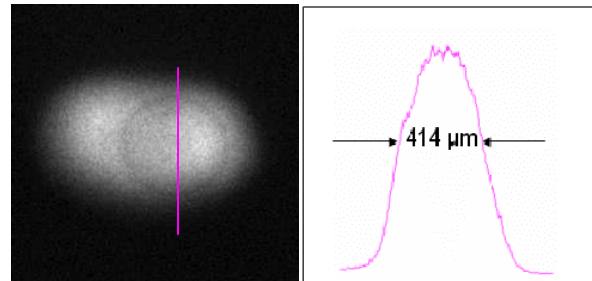


FIG.1. Image of Ti K-alpha emission and lineout showing fwhm on the vertical axis with radiograph of early stage of imploding shell.

The single hit CCD spectrum was extracted as a pixel count histogram and the image thermal and Bremsstrahlung background were subtracted. The peak of this spectrum was then assigned the 4.5 keV K α emission energy as illustrated in figure 2. The number of K α photons was deduced by integrating this line. The absolute photon number was obtained by taking into account filter transmission, CCD quantum efficiency (~ 0.6), single hit probability (~ 0.5), and the solid angle subtended by the analyzed area of the CCD. Thus,

photons per steradian yield at 41° from axis normal were obtained for each shot.

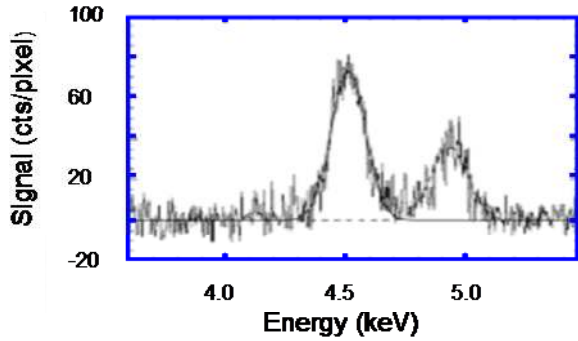


FIG.2. Single hit CCD spectra of Ti $K\alpha$ and $K\beta$

The imaging CCD outputs a 1024×1024 array of 16 bit numbers. This allowed us to obtain a relative intensity map of the $K\alpha$ data. FWHM areas were combined with absolute $K\alpha$ yield to find source brightness. A uniform 450 count thermal background was subtracted and the images were integrated to find a relative $K\alpha$ yield. Figure 3 shows a plot of this relative $K\alpha$ yield against the absolute $K\alpha$ yield from the CCD spectrometer. At low yields, a trend line indicates a linear relationship and gives an absolute calibration of the imager. However, at high yield the data points are significantly to the right of the trend line.

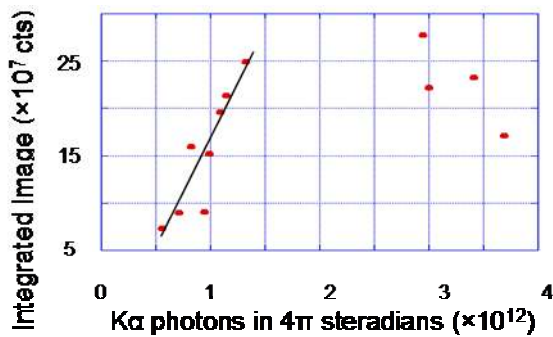


FIG.3. Integrated image intensity vs. $K\alpha$ yield. Trend line for low yield data points shows linear proportionality and its slope gives an absolute calibration of the image brightness.

The average total yields for the low and high yield sets of data are 9.5×10^{11} and 3.3×10^{12} photons with average laser energy of 50J. The $K\alpha$ conversion efficiencies are then 1.4×10^{-5} and 4.9×10^{-5} , respectively. These results can be compared with published data for an experiment³ at 2×10^{16} W/cm² which gives a conversion of 1.1×10^{-4} . Monte Carlo modeling⁴ for the same intensity gives a conversion of 7.5×10^{-4} . The order of magnitude higher efficiency is associated with the models assumption of 50% conversion of laser energy to electrons which is not supported by our data. A possible explanation of the two different behaviors is differences in pre-plasma formation. There is variability in the ASE (amplified spontaneous emission) pedestal

level of the laser. The ASE energy in a few nanoseconds before the pulse is about 1 J/cm². This is very close to the plasma formation threshold of a metal surface so that relatively small variations in the ASE can lead to larger variations in the preformed plasma present in front of the metal before the main pulse. Significant variations in the hot electron conversion efficiency and the $K\alpha$ production can therefore ensue.

Average laser intensity was obtained from the $K\alpha$ spot FWHM area on the imager. The hot electron temperature was estimated from classical resonance absorption, as confirmed by Beg et al.⁵ with the scaling, $T_{hot} = 100 \text{ keV} * I^{1/3}$, where I is units of 10^{17} W/cm². The resulting source temperature of 57keV at the average intensity of 1.9×10^{16} W/cm² was used for the electron source in Monte Carlo simulations.

A model employing the electron/photon Monte Carlo transport code ITS⁶ simulated $K\alpha$ emission from the Ti foil. Electrons were injected into a circular irradiated area equal to the experimental area with a Boltzmann electron energy spectrum of 57 keV and a 26 degree cone angle. The $K\alpha$ production was computed on the back surface of the foil and summed per steradian as a function of view angle. The results are plotted in fig. 4. Also shown for comparison are the results of an isotropic injection of electrons. A value of 5.0×10^{-4} photons/sr per electron at the relevant 41° view angle was obtained by the model. The photons per steradian at 41° were measured by the single hit CCD. The resulting mean values are 7.6×10^{10} photons/sr from the main set of data and 2.6×10^{11} photons/sr from the high yield data. The average numbers of 57 keV electrons for the two sets of data are therefore 1.5×10^{14} and 5.2×10^{14} . This results in respective laser to electron conversion efficiencies of 3% and 10%. As argued previously, this variation in electron conversion efficiency may arise from small variations in the ASE laser pre-pulse.

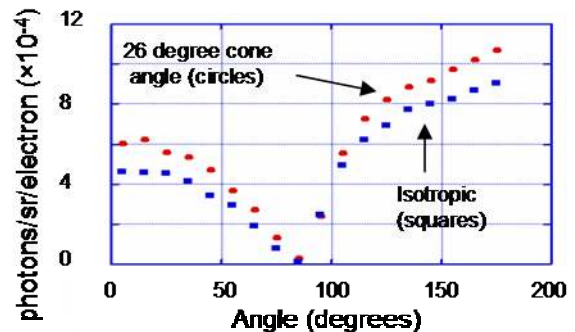


FIG.4. Monte Carlo modeling of $K\alpha$ yield vs angle from a 25 micron thick 1 mm diameter Ti foil.

Increased electron conversion efficiency can also lead to ionization induced shifts of the $K\alpha$ line⁷ which can be sufficient to shift the line outside the bandwidth of the crystal imager (defined by the range of angles of incidence included in its aperture). Line shift as a function of Ti atom ionization has been calculated using

a multi-configuration Dirac-Fock (MCDF) model^{8,9}. The average ion charge for a given energy density of solid density Ti in local thermodynamic equilibrium (LTE) was obtained from Los Alamos equation of state library tabulations (Sesame tables). An analytic model of energy deposition by supra-thermal electrons¹⁰ provided the energy density as a function of target depth for a given laser intensity and conversion efficiency.

The crystal Bragg angle for cold $K\alpha_1$ is 1.0° and this line is reflected by the crystal over a spatial band whose width is determined by the natural linewidth and the curvature and rocking curve of the crystal. The spherical surface spanned angles of incidence from 0° to 2° . The energy shift of the $K\alpha$ line with increased ionization initially goes negative to a maximum shift of $\Delta E = -1.74$ eV for $Z = 5$ ionization, then positive. At the crystal, a negative shift of $\Delta E = -0.93$ eV, for an ionization $Z = 4.4$, reduces the Bragg angle to 0° . For greater negative shifts the crystal no longer reflects. We constructed a model giving the $K\alpha_1$ collection efficiency of the crystal (relative to cold $K\alpha_1$) as a function of the energy shift and thus as a function of foil depth. The product of $K\alpha$ yield, crystal collection efficiency and attenuation through the material was summed over all depths and divided by the total $K\alpha$ yield to give the reduction of collected $K\alpha$ due to ionization state shifting. Figure 5 shows this relative collection efficiency vs. electron conversion efficiency for a hot electron temperature corresponding to an intensity of $1.9 \times 10^{16} \text{ W/cm}^2$. The plot shows a reduction from $\sim 100\%$ to $\sim 80\%$ for an increase in conversion efficiency from $\sim 3\%$ to $\sim 10\%$. The discontinuity in the data in figure 3 therefore may be partially explained by a decrease in conversion efficiency associated with the pre-pulse ionization of the Ti target as discussed previously.

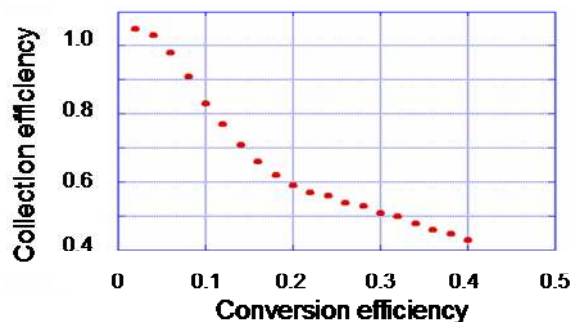


FIG. 5. For increased conversion efficiency more target heating occurs. As a result, a significant number of K-alpha photons are state shifted beyond the crystal bandwidth and the collection efficiency is reduced.

The crystal imager is expected to have an integral reflectivity¹¹ of 1.875×10^{-3} radians. Its effective reflectivity depends on the source bandwidth relative to the bandwidth of the crystal aperture, accounting for varying angles of incidence across the crystal surface¹². For our instrument, the geometrical bandwidth is larger than the source bandwidth, and so the effective

reflectivity is determined by the integral reflectivity divided by the geometrical bandwidth. This suggests an effective reflectivity of 5.7%

A calculation was made to estimate the actual effective reflectivity of our imager. The count response of the imaging CCD for single hit photons was measured by looking at the count histogram in the low exposure part of the image. After subtraction of thermal background, a peak due to $K\alpha$ was observed at 209 ± 8 counts. A total reflected photon number was then calculated from the integrated CCD intensity, accounting for the quantum efficiency (0.2 ± 0.1), the transmission of the filters, and the solid angle subtended by the crystal. The effective reflectivity was this total $K\alpha_1$ photon number divided by the absolute $K\alpha_1$ photon count data from the spectrometer. The spectrometer cannot resolve $K\alpha_1$ and $K\alpha_2$ and so a correction was made to the number of collected single hit photons. The correction factor of $2/3$ was used because the relative intensity of $K\alpha_1$ is twice that of $K\alpha_2$ ¹³. Excluding the four high yield shots, the effective crystal reflectivity is $3.75 \pm 2\%$, which is within a factor of two of the expected reflectivity.

The authors gratefully acknowledge the efforts of R. Clarke, M. Notley, R. Heathcote, D. Neville, P. Brummitt, M. Tolley and D. Neely. This work was performed under the auspices of the U.S. Department of Energy by the University of California Lawrence Livermore National Laboratory under contract No. W-7405-Eng-48. The work was supported by United Kingdom's Engineering and Physical Sciences Research Council and the Council for the Central Laboratory of the Research Councils.

¹ J King et al., in *Inertial Fusion Sciences and Applications 2003 (IFSA)*, edited by B.A. Hammel, D.D. Meyerhofer, J. Meyer-ter-Vehn, and H. Azechi, (Monterey, Calif., 2003), pp. 449-452

² J.A. Koch, Y. Aglitskiy, C. Brown, R. Freeman, S. Hatchett, G. Holland, M. Key, A. MacKinnon, J. Seely, R. Snavely, R. Stephens, *Rev. Sci. Instrum.* **74**, 2130 (2003).

³ Ch. Reich, I. Uschmann, F. Ewald, S. Dusterer, A. Lubcke, H. Schwoerer, R. Sauerbrey, E. Forster, *Phys. Rev. E* **68**, 056408 (2003).

⁴ Ch. Reich, P. Gibbon, I. Uschmann, E. Fortster, *Phys. Rev. Letts.* **84**, 4846 (2000)

⁵ F.N. Beg, A.R. Bell, A.E. Dangor, C.N. Danson, A.P. Fews, M.E. Glinsky, B.A. Hammel, P. Lee, P.A. Norreys, M. Tatarakis, *Phys. Plasmas* **4**, 447 (1997).

⁶ J. A. Halbleib and T. A. Mehlhorn, "ITS: The Integrated TIGER Series of Coupled Electron/Photon Monte Carlo Transport Codes," Sandia National Lab Report No. SAND84-0573, November 1984

⁷ E. Martinolli, M. Koenig, J.M. Boudenne, E. Perelli, D. Batani, T.A. Hall, *Rev. Sci. Instrum.* **75**, 2024 (2004).

⁸ M. H. Chen, *Phys. Rev. A* **31**, 1449 (1985)

⁹ I. P. Grant, B. J. McKenzie, P. H. Norrington, D. F. Mayers and N. C. Pyper, *Comput. Phys. Commun.* **21**, 207 (1980).

¹⁰ R.J. Harrach and R.E. Kidder, *Phys. Rev. A* **23**, 887, (1981)

¹¹ J. Seely, Naval Research Laboratory, Personal Communication.

¹² J. A. Koch, *Applied Optics* **37**, 1784 (1998)

¹³ Thompson, A.C., *et al.*, *X-ray Data Booklet*, 2nd ed., Berkeley, Ca., Lawrence Berkeley National Laboratory, 2001